Strength and toughness of biocomposites consisting of soft and hard elements: A few fundamental models

Ko Okumura

Certain biocomposites exploit the combination of soft and hard elements to achieve high strength and toughness. In nacre, found inside certain seashells or on the surface of pearls, hard layers of micron-scale thickness are glued together by thin layers of soft proteins to realize remarkable strength and toughness. In spider webs, stiffer radial threads are connected by softer spiral threads to produce a light and resistant structure. In the exoskeleton of lobsters, organic fibers form a chiral structure in an inorganic matrix. This article reviews progress in the understanding of the mechanical superiority of such soft-hard biocomposites. In particular, simple physical views are presented that allow an intuitive understanding of how their remarkable structures contribute to enhancing their fracture resistance in the presence of cracks, and how such structures are physically optimized in terms of mechanical properties. Such fundamental insights could be useful as guiding principles for developing artificial, reinforced materials.

Introduction

In nature, there are strong and tough biological materials that often possess remarkable hierarchical structures.[1–4] Examples of such natural materials include nacre, the exoskeleton of crustaceans, and spider webs. Using these examples, we emphasize the role of simple models for structures, which yield physical insights and often reveal useful scaling laws.

A scaling law gives an important physical quantity as a product of the powers of other physical parameters, as in Equations 1 and 2 given later in the text. Scaling laws are useful as guiding principles for various applications such as industrial development of reinforced materials, although they are mathematically exact only in the limit in which a number of physical parameters, X, Y, . . ., are much larger or smaller than certain values. Such a limit is often expressed as a set of inequalities, such as $X >> X_0$ and $Y << Y_0$.

In general, when a scaling law is obtained, its validity can be established through "data collapse." A clear example is shown in **Figure 1**e: The original three scattered curves on the left fall onto a single curve on the right as a result of replotting the same data on new axes. The quantities used for the new x and y-axes are obtained by rescaling the quantities used for the original x and y axes in a way specified by the underlying scaling law shown in Figure 1e. (Figure 1d demonstrates another example of the data collapse.) Theoretically, scaling laws become exact only in a limit as stated previously. However, scaling laws are frequently valid in a practical sense over wide parameter ranges far beyond the theoretical restriction. Accordingly, scaling laws could be guiding principles for the development of various products in industries, such as new reinforced materials.

To understand strength and/or toughness of materials for reinforcement, it is important to know the locations at which the stress field is locally enhanced when an external load is applied. Stress is concentrated at the tips of cracks or flaws, and such a concentrated tip stress can trigger failure of materials. Accordingly, it is indispensable to know how stress is concentrated, in particular when a simple line crack is present, as shown later in this article.

Nacre

Nacre is a strong biological material and possesses a magnificent hierarchical structure. It has been actively studied[5–8] together with, for example, bone,[9–11] and has inspired a number of artificial materials.[12–17] In nacre, the layered structure is composed of hard plates of aragonite and soft layers of proteins[5] (see Figure 1a). Although soft layers are much thinner than hard layers, the fracture surface energy of nacre is a few thousand times as high as that of a monolith of hard aragonite.[18] A number of different mechanisms for the toughness

Ko Okumura, Department of Physics, Ochanomizu University, Japan; okumura@phys.ocha.ac.jp
DOI: 10.1557/mrs.2015.66

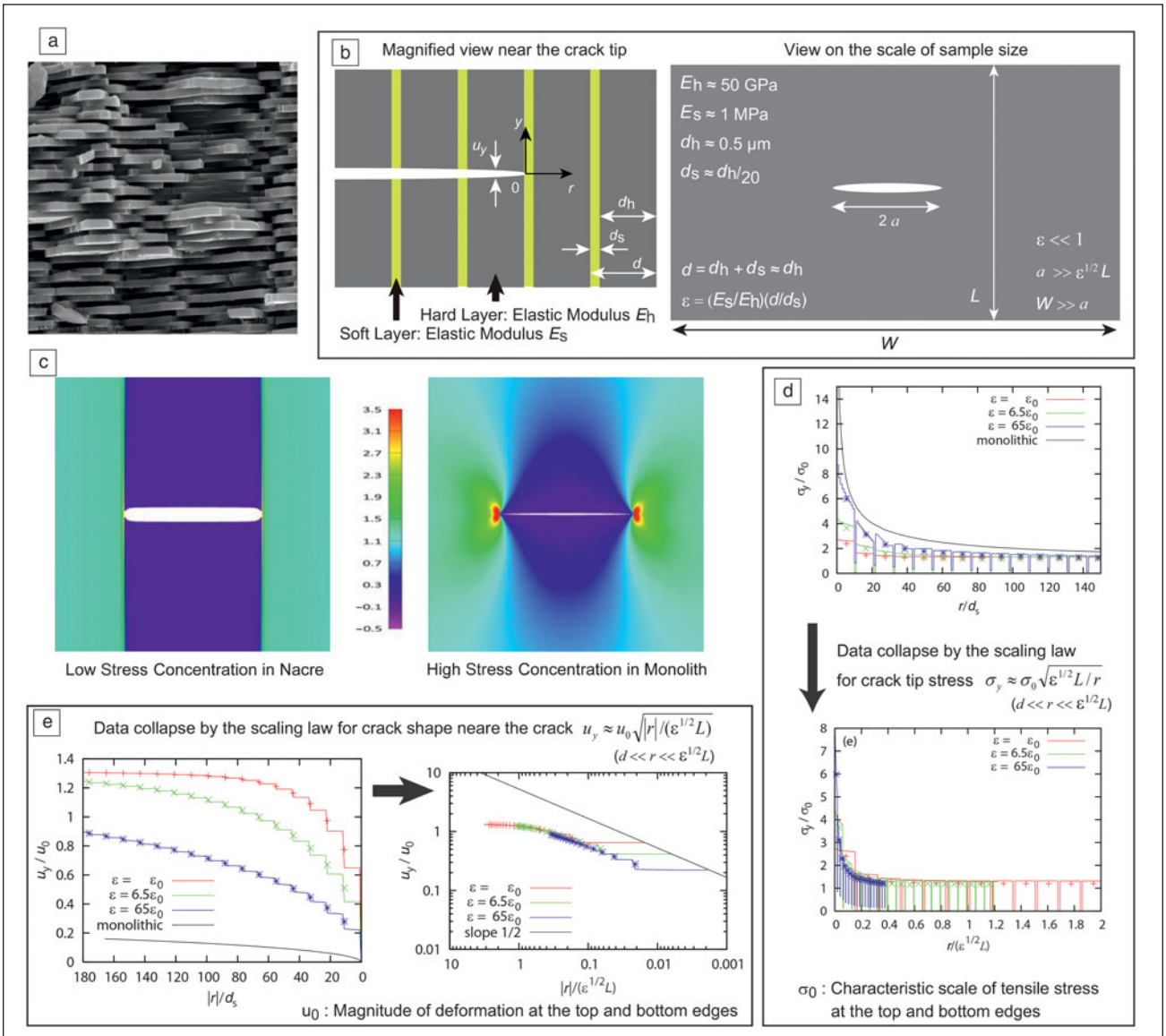

Figure 1. (a) Scanning electron microscope image of the section of nacre. The thickness of hard layers is approximately 0.5 μm. Because the soft layers are extremely thin (approximately 25 nm), they cannot be seen. (b) Illustration of a simplified model of nacre with a crack and structure parameters in the model. The left-hand illustration is drawn on the scale of layered structure, while the right-hand is drawn on the sample scale. (c) Stress distribution under the presence of a line crack in a plate of nacre (left) and a monolith of the hard element of nacre (right) with an intensity scale (middle), obtained by finite element calculations. Stress concentration near the crack tips is significantly reduced in nacre. (d) The top plot shows stress distribution around the right crack tip (b) of a horizontal line crack. Stress values are more reduced for smaller ε (the case $\varepsilon = \varepsilon_0$ corresponds to real nacre). The bottom plot shows collapse of the same data by rescaling of the axes, confirming the validity of the scaling law shown in the panel. (e) Crack shape near the tip (left) and collapse of the data (right), confirming the scaling law shown in the panel. The plots show that the deformation is more enhanced for smaller ε_0. (a) Courtesy of Prof. Dinesh Katti. (c–e) Created from data in Reference 37.

and strength of nacre have been pointed out on the basis of experimental observations: Soft layers are elongated in a stepwise way when stretched;[19] thin compressive layers between hard layers lead to a remarkable strength;[20] layer interfaces are rather rough;[21] mineral bridges are found between layers;[22] and the surface of hard plates are wavy.[23] Numerous theoretical studies have also been attempted, including studies using (1) elastic models[20] based on analytical solutions[24,25] and scaling arguments,[26,27] (2) viscoelastic models,[28] (3) micromechanical models,[29] and (4) numerical models such as finite-element models,[23,30,31] a fuse network model,[32] and a model with a periodic Young's modulus.[33]

The model discussed in Reference 24 is a simple layered structure of hard and soft plates, mimicking the structure of nacre as shown in Figure 1b. The model is based on the elastic moduli for soft and hard layers, E_h and E_s, respectively, and the thicknesses for soft and hard layers, d_h and d_s, respectively. These parameters satisfy the following relations: $E_h >> E_s$

https://doi.org/10.1557/mrs.2015.66 Published online by Cambridge University Press

and $d_h >> d_s$. The elastic energy of this simple model can be constructed in the limit of small ε under the existence of a line crack perpendicular to the layers, where ε is defined as $\varepsilon = (E_s/E_h)(d/d_s)$ with $d = d_h + d_s$. Reasonable values of the parameters are $d_h = 0.5$ μm, $d_s = d_h/20$, $E_h = 50$ GPa, and $E_s = 1$ MPa (the soft layers are like gels[34]); for this set of parameters, ε is significantly small ($\varepsilon \sim 10^{-4}$). When the sample is stretched in the y direction, on the basis of the elastic energy in the small ε limit, the dominant component of deformation field u_i and stress field σ_{ij} are shown to be u_y and σ_{yy} (termed σ_y in the following), with the other components being negligibly small in comparison.

In addition, the dominant component of the deformation field u_y was shown to be governed by an anisotropic Laplace equation.[24] The equation for u_y can be analytically solved under boundary conditions. For example, the conditions that describe a line crack of length $2a$ propagating in the r direction, as illustrated in Figure 1b,[24,35] are specified in the following way: The stress σ_y is zero at the surface of the crack (i.e., at $y = 0$ and $-a < r < a$), the deformation u_y is zero at $y = 0$ from symmetry, except for the region $-a < r < a$ in which the crack is located. The fixed grip condition is specified by the requirements that the deformation u_y is set to $u_y = u_0$ and $-u_0$ at the top and bottom edges (i.e., $y = L/2$ and $-L/2$ where L is the height of the sample as defined in Figure 1b). With these boundary conditions, a complete analytical solution for u_y is obtained via a special conformal mapping augmented by a transformation for avoiding the singularity that appears on the $y = 0$ axis.

The analytical solution of the stress field σ_y is obtained from that of u_y. Near the crack tip ($|r| << \varepsilon^{1/2}L$), the analytical solutions give the following scaling laws for the deformation and stress fields at $y = 0^+$ (the symbol 0^+ implies the limit $y \to 0$ from a positive y):

$$u_y \approx u_0\sqrt{|r|/(\varepsilon^{1/2}L)} \text{ for } r < 0, \tag{1}$$

and

$$\sigma_y \approx \sigma_0\sqrt{\varepsilon^{1/2}L/r} \text{ for } r > 0, \tag{2}$$

where L is the sample height and σ_0 is a characteristic size of the stress at the top and bottom edges (at $y = L/2$ and $-L/2$). The above scaling laws predict that, compared with a monolith of aragonite, stress concentration is reduced by the factor $\varepsilon^{1/4}$ and deformation is enhanced by the factor $\varepsilon^{-1/4}$. Theoretically, these scaling laws are valid under the following conditions:

$$\varepsilon << 1,\ d << r << \varepsilon^{1/2}L << a << W. \tag{3}$$

The reduction in stress concentration predicted previously[24] has been confirmed by numerical calculations,[36,37] as shown in Figure 1c. In addition, numerical results provide physical insights, as suggested in Figure 1d–e: As ε gets smaller, as in nacre, soft layers are stretched all the more and, correspondingly, the deformation of the hard layers is reduced. As a result, the stress near the crack tip, which is governed by the hard layers, is reduced.[36,38]

Finite element calculations[37] revealed that the simple scaling laws derived in Reference 24 are robust. Namely, the laws are valid over wide parameter ranges far beyond the theoretical requirements by a clear "data collapse." In Figure 1e, the scattered curves on the left are collapsed onto a single master curve, as seen on the right. Figure 1d also demonstrates a data collapse.

Some of the collapsed data include the data obtained in cases that break the required conditions, which suggests the robustness of the scaling laws. In fact, many conditions specified in Equation 3 are required for the scaling laws to be valid theoretically, but, in the simulations, the conditions $d << r << \varepsilon^{1/2}L << a << W$ are significantly relaxed (e.g., $W/a = 3$ for all cases of ε) and the condition $\varepsilon^{1/2}L << a$ is violated in the case $\varepsilon = 65\varepsilon_0$ with $\varepsilon_0 = 6500$ (the case of $\varepsilon = \varepsilon_0$ corresponds to real nacre); nonetheless, agreements between theory and simulation are remarkable.

In Reference 24, a scaling law for the fracture energy of the model nacre, a measure of fracture toughness, is also derived under the condition given in Equation 3 on the basis of Equations 1 and 2:

$$G_c \approx \varepsilon^{-1/2}(d/a_0)G_h, \tag{4}$$

where the large enhancement factor for the fracture energy, which is expressed as

$$\varepsilon^{1/2}(d/a_0) = \sqrt{E_h/E_s}\sqrt{d_s/d_h}(d/a_0), \tag{5}$$

is consistent with experimental values.[18] Here, G_h is the fracture energy of the monolith of brittle aragonite ($G_h \approx 1$ J m^{-2}) and a typical defect size in hard layers a_0 is of the order of the thickness of soft layer d_s ($a_0 \approx 0.5/20$ μm = 0.025 μm), which lead to the following conclusion: G_c is a few 1000 J m^{-2}.

In summary, concerning the simple model of nacre, scaling laws for the crack tip stress and the crack shape given in Equations 1 and 2 are obtained analytically and confirmed by numerical calculations via clear data collapse. In fact, another scaling law for the maximum stress that appears at the crack,

$$\sigma_M \approx \sigma_0\sqrt{\varepsilon^{1/2}L/d} \text{ for } r > 0, \tag{6}$$

is derived and confirmed by numerical calculations.[37,39,40] On the bases of the three established scaling laws, Equation 4 is derived, which has been indirectly confirmed but has yet to be directly or experimentally confirmed. Ranges of the validity of scaling laws thus proposed are theoretically limited by the conditions in Equation 3, which are also enumerated in Figure 1. However, numerical calculations again suggest that the scaling laws are practically valid over wide parameter ranges far beyond the theoretical restriction.

https://doi.org/10.1557/mrs.2015.66 Published online by Cambridge University Press

Equation 4 leads to some guiding principles for reinforcing soft-hard layer composites, which suggest that the structure of nacre is rather optimized. For example, large values of d/a_0 ($\sim d_h/d_s$) and E_h/E_s as observed in nacre are advantageous for toughening, as predicted by Equation 4.

Exoskeleton of crustaceans

The exoskeleton of crustaceans is composed of inner and outer layers known as the endocuticle and exocuticle, respectively.[41] Both layers possess a remarkable helical structure (**Figure 2**a) but with different helical pitches: bundles of chitin-protein fibers are embedded in a calcium carbonate matrix with the bundles forming a chiral structure. This structure is universal in crustaceans,[42] but its mechanical properties have been studied only recently,[43,44] including studies using artificial biomineralization to mimic the chiral structure.[45–47]

By noting that the fiber bundles are softer than the matrix, the helical structure has been mapped into a layered structure of soft and hard layers of equal thickness, where each layer is a composite of fiber bundles and matrix (as illustrated in Figure 2b).[48] For example, when the sample is stretched in the y direction, as in Figure 2a–b, in the layers numbered 0, 6, 12, and 18, which are a composite of fibers and matrix, fiber direction is parallel to the stretch direction, rendering these layers stronger than the layers numbered 3, 9, and 15, in which the fiber direction is perpendicular to the stretch direction. In other words, the elastic modulus periodically changes along the z-axis when the sample is stretched in the y direction. As a result, on the length scale of the spiral pitch, the structure can be approximately regarded as a layered structure as in the right-hand illustration in Figure 2b.

This structure is similar to the structure of nacre except for (1) the thickness of soft and hard layers are approximately the same ($d \approx d_s \approx d_h$), and (2) E_h and E_s are determined to be functions of the elastic moduli of the matrix and bundle, E_m and E_b, and the volume fractions of the matrix and bundles, φ_m and φ_b (for different approaches to the periodically changing elastic modulus, see References 33 and 49–52). The volume fractions can be conveniently parameterized by introducing a small parameter δ where $\varphi_m = (1 + \delta)/2$ and $\varphi_b = (1 - \delta)/2$, because φ_m is approximately equal to φ_b in living lobsters, and the volume fractions satisfy the relation $\varphi_m + \varphi_b = 1$.

For this simplified layered structure of the exoskeleton, all four scaling laws, Equations 1, 2, 4, and 6, established for the nacre model, can be exploited if the small parameter ε in these scaling laws is replaced with $\varepsilon = [(1 + \delta)(1 - \delta)E_m/E_b]-1$ for the exoskeleton in order to reflect the substructure of fiber bundles and matrix. This is possible because the laws derived for nacre are valid as long as the conditions given in Equation 3 are satisfied. The enhancement factor $\varepsilon^{-1/2}(d/a_0)$ for the fracture energy in Equation 4 can be expressed as:

$$\varepsilon^{1/2}(d/a_0) \approx \sqrt{(1+\delta)(1-\delta)E_m/E_b}\,(d/a_0) \text{ for } E_m > E_b. \quad (7)$$

In addition, when Equation 4 is applied to the exoskeleton, G_h is the fracture energy in the toughest direction of a parallel composite in which fiber bundles are oriented parallel to each other throughout the matrix rather than helically. The fracture strength and toughness of this parallel composite is direction-dependent and is strongest when under tension in the direction of the bundles.

The enhancement factor for the fracture energy given in Equation 7 for the exoskeleton is estimated to be a few 1000, which is similar to nacre. This is because in the case of the exoskeleton, the period of the structure d ($\approx 2d_s$ as $d_s \approx d_h$) corresponds to the helical pitch p ($\approx$50 μm) and a_0 to the bundle diameter ($\approx$0.5 μm). Here, rather rough approximations have been utilized for the elastic moduli: The elastic

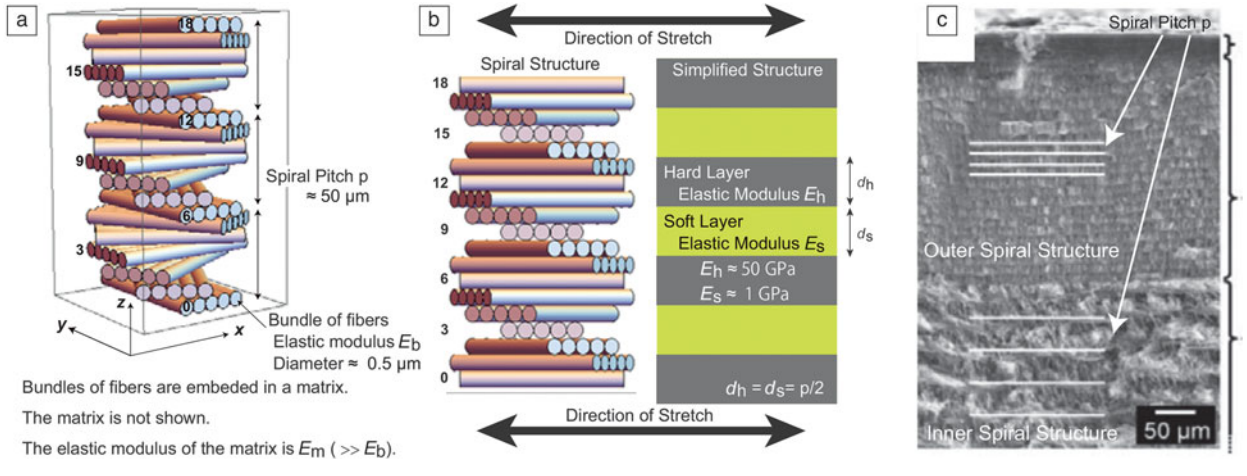

Figure 2. (a) Illustration of the spiral structure of cuticle layers in the exoskeleton of lobsters, generated by Mathematica 10 software. The layers are numbered from 0 to 18. (b) Original spiral structure (left), and its simplified layered structure (right) when the sample is stretched in the specified direction. The layer numbers correspond to those in (a). (c) Scanning electron microscope image of outer and inner spiral structures (exocuticle and endocuticle) with different spiral pitches, observed in the exoskeleton of lobsters. (c) Reproduced with permission from Reference 41. © 2009 Wiley.

https://doi.org/10.1557/mrs.2015.66 Published online by Cambridge University Press

modulus of the matrix (amorphous calcium carbonate) is approximately 50 GPa, and that of the bundles (a composite of chitin fibers and proteins) is around 1 GPa.

By comparing the two enhancement factors in Equations 5 and 7, some differences are noticed in the strategy used for increasing the corresponding enhancement factor for the fracture energy. In nacre, the factor $\sqrt{E_h/E_s}$, dominates over the other factors, whereas the factor d/a_0 dominates in the exoskeleton. In other words, the combination of extremely soft and hard is exploited in nacre, whereas in the exoskeleton case, the substructures (i.e., the bundles and matrix) are effectively used to adjust helical pitches to enlarge the factor d/a_0 and achieve roughly the same order of fracture toughness. Adjusting the helical pitch has another advantage, which is discussed later.

In the case of the exoskeleton, confirmation of the four scaling laws (for the stress and deformation fields, the maximum stress, and the fracture energy) by experiment or simulation is still under way, however, Equation 4 and Equation 7 support the fact that the following features observed in the exoskeleton are mechanically advantageous. These features can be regarded as guiding principles for toughening, as also supported by theory: (1) The combination of soft and hard elements (i.e., $E_b < E_m$); (2) the helical structure, because of which the fracture energy becomes even larger than that in the toughest direction of the parallel structure; (3) the equal volume fractions of the matrix and bundle, which correspond to a sharp peak in the enhancement factor in Equation 7 when δ is zero (i.e., when $\varphi_m = \varphi_b$); and (4) the exocuticle with a small helical pitch covers the endocuticle with a large helical pitch, contributing to the reinforcement of the structure in the following manner: A helical structure with a long pitch d cannot be protected against small cracks because Equation 7 is valid for a crack whose size a is larger than d, as suggested in Equation 3. Thus, the exocuticle protects the inside from smaller cracks (but with a lower toughness than the endocuticle), while the endocuticle protects the inside from larger cracks (with a higher toughness than the exocuticle).

Spider webs

Spider silks are high-performance polymeric fibers and thus have been actively studied over the years[53,54] in terms of their entropic elasticity,[55] water coating,[56] breaking strength,[57] gene family,[58] liquid-crystalline structure,[59] micellar structure,[60,61] hierarchical structure,[62] and torsional relaxation.[63] The mechanical advantages of spider webs have yet to be explored, except for studies on structural vibration,[64,65] tensile pre-stress,[66] detailed finite-element modeling,[65,67] and nonlinear response.[68–70]

A simple model of orb spider webs is composed of stiff radial and soft spiral threads and is under a global strain,[71] as in real spider webs[67] (see **Figure 3**a–b). It is convenient to introduce a specific spring constant as the spring constant multiplied by the length of the spring (the spring constant is inversely proportional to the length). This quantity can be expressed as the elastic modulus multiplied by the section area

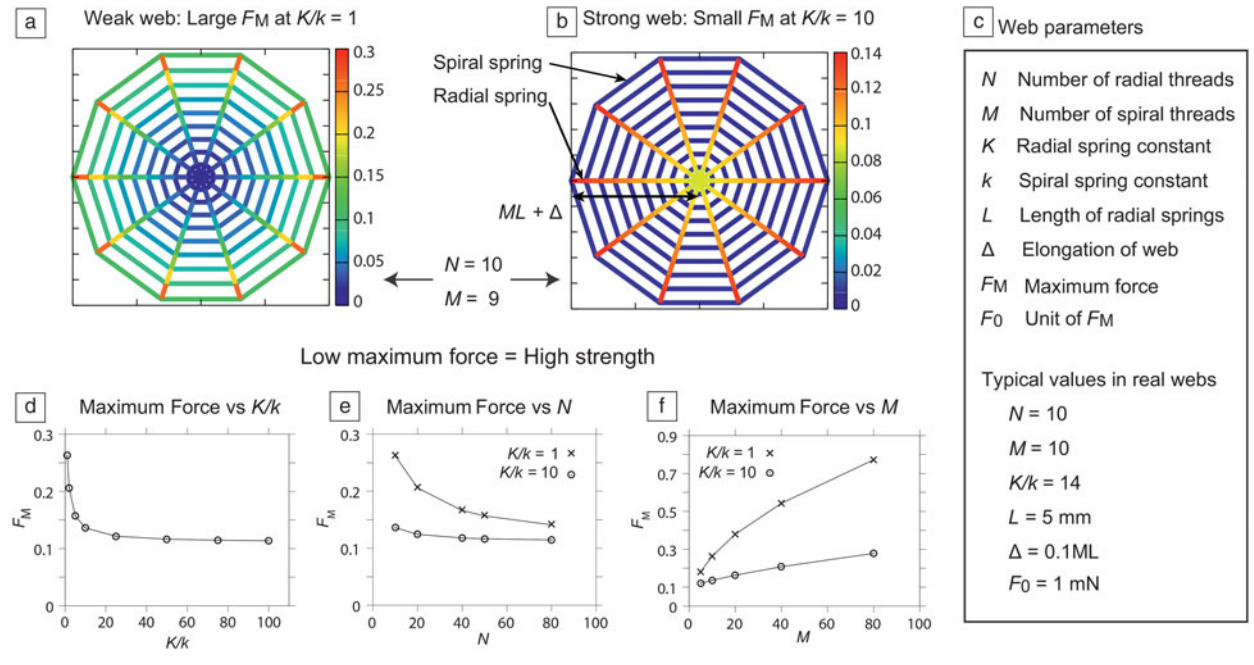

Figure 3. (a–b) Force distribution in a simple model of spider webs under tension. The ratio of radial thread and spiral thread spring constants (multiplied by the length) of (a) and (b) are K/k = 1 and 10, respectively. The maximum force F_M that appears at the edge radial thread is smaller in (b), which suggests that real webs (corresponding to [b]) are stronger than artificial webs in which K is comparable to k. (c) Summary of parameters in the model spider web. (d–f) The maximum force F_M as a function of K/k, the number of radial threads N, and the number of spiral threads M, respectively. The three plots show that higher K/k values are mechanically advantageous. (a–b) and (d–f) Created from data in Reference 71.

https://doi.org/10.1557/mrs.2015.66 Published online by Cambridge University Press

of a thread to compare the relative stiffness of the threads. The specific spring constants for the radial and soft threads are denoted K and k, respectively. Typical values of the diameter, elastic modulus, and initial tension of radial threads are 3.9 μm, 1 GPa, and 0.13 mN, respectively, and those of spiral threads are 2.4 μm, 0.8 GPa, and 10 μN, respectively.[67] These numbers are consistent with other typical values shown in Figure 3c.

As demonstrated in Figure 3a and b, the model web is stronger, that is, a maximum force F_M appearing in a web is smaller, when the stiffness contrast K/k is larger than one; as in real webs. Here, the maximum force F_M is considered to be a measure of strength, because in general, materials start failing at the position where a strong local force acts.

The simple model of spider webs further reveals surprising conclusions, although the model predicts no scaling laws. The stiffness ratio K/k seems to be optimized in real webs from a number of mechanical viewpoints, giving high adaptability to spiders: (1) In Figure 3d, the maximum force F_M sharply drops in a range of small K/k but changes little when K/k is larger than around 14, which is a typical value of the stiffness difference in real webs.[67] Considering the difficulty for spiders to create two types of thread whose mechanical properties are quite different, the typical value of the stiffness difference of 14 may be regarded as a result of optimization. (2) The weak dependence of the maximum force F_M on the number of radial threads N and that of spiral threads M for large K/k (Figure 3e–f, respectively) suggests spiders can be highly flexible to improve their chances of survival. Spiders can spin webs by freely selecting the number of spiral and radial threads, according to the spatial and biological environments, for example, to a typical branch spacing of trees or to a typical size of prey. (3) This model also explains how spider webs function well even if some parts of spiral threads are missing. Remarkably, stress concentration is absent in spider webs.

Conclusion

A key feature in the reinforcement on the three biological materials discussed here, nacre, the crustacean's exoskeleton, and spider webs, is the combination of soft and hard elements. Simple models reveal that the structures are optimized in a number of mechanical senses, and simple scaling laws or simple physical understandings provide guiding principles for developing tough materials mimicking the biological structures. It is possible that such a naive model is oversimplified and fails to capture the reality of the original material. Even in such a case, simple guiding principles obtained from a biologically inspired study are useful in their own right and could lead to the development of an artificial material that is even stronger than the original biological material. This fact further justifies the importance of studies on complex systems via simple models.

An extreme example of soft-hard composites is porous materials with voids corresponding to the soft element. In fact, there are many porous and strong materials in nature, such as the stereom of holothurians (e.g., the soft bone of sea cucumbers),[72] the skeleton of a certain sponge,[73] and the frustules (hard cell walls) of diatoms.[74] Accordingly, studies on reinforcement with voids would be an interesting direction of research.[75,76] Nonlinear extension of the simple models would also play an important role in the future study of biological materials and biomaterials.[39,40,77]

Approaches via a simple model, often using scaling laws, are promising and have been accepted, especially in fields in which engineering or material scientists meet physicists, for example, in polymer science,[76,78] wetting,[79,80] and granular physics.[81,82] This review will be useful for disseminating the perspective of physicists for complex systems in fields in which such simple approaches have yet to be used, including fields concerning fracture and toughness of materials.

Acknowledgments

This research was supported by Grant-in-Aid for Scientific Research on Innovative Areas, "Fusion Materials (Area no. 2206)," of MEXT, Japan, by a Grant-in-Aid for Scientific Research (A) (No. 24244066) of JSPS, Japan, and by the ImPACT Program of the Council for Science, Technology and Innovation (Cabinet Office, Government of Japan).

References

1. M.A. Meyers, A.Y. Lin, Y. Seki, P.-Y. Chen, B.K. Kad, S. Bodde, *JOM* **58**, 35 (2006).
2. P. Fratzl, R. Weinkamer, *Prog. Mater. Sci.* **52**, 1263 (2007).
3. B. Ji, H. Gao, *Ann. Rev. Mater. Res.* **40**, 77 (2010).
4. J. Vincent, *Structural Biomaterials* (Princeton University Press, New Jersey, 2012).
5. M. Sarikaya, J. Liu, I. Aksay, *Biomimetics: Design and Processing of Materials* (AIP, New York, 1995), pp. 35–90.
6. S. Kamat, X. Su, R. Ballarini, A. Heuer, *Nature* **405**, 1036 (2000).
7. H. Gao, B. Ji, I. Jäger, E. Arzt, P. Fratzl, *Proc. Natl. Acad. Sci. U.S.A.* **100**, 5597 (2003).
8. G. Mayer, *Science* **310**, 1144 (2005).
9. J.D. Currey, *Bones: Structure and Mechanics* (Princeton University Press, New Jersey, 2002).
10. P. Fratzl, H. Gupta, E. Paschalis, P. Roschger, *J. Mater. Chem.* **14**, 2115 (2004).
11. C. Hellmich, J.-F. Barthélémy, L. Dormieux, *Eur. J. Mech. A Solids* **23**, 783 (2004).
12. T. Kato, *Adv. Mater.* **12**, 1543 (2000).
13. M. Sarikaya, C. Tamerler, A. Jen, K. Schulten, F. Baneyx, *Nat. Mater.* **2**, 577 (2003).
14. S. Deville, E. Saiz, R. Nalla, A. Tomsia, *Science* **311**, 515 (2006).
15. E. Munch, M. Launey, D. Alsem, E. Saiz, A. Tomsia, R. Ritchie, *Science* **322**, 1516 (2008).
16. L. Bonderer, A. Studart, L. Gauckler, *Science* **319**, 1069 (2008).
17. L. Corte, L. Leibler, *Macromolecules* **40**, 5606 (2007).
18. A. Jackson, J. Vincent, R. Turner, *Proc. R. Soc. Lond. B* **234**, 415 (1988).
19. B. Smith, T. Schäffer, M. Viani, J. Thompson, N. Frederick, J. Kindt, A. Belcher, G. Stucky, D. Morse, P. Hansma, *Nature* **399**, 761 (1999).
20. M.P. Rao, A. Sanchez-Herencia, G. Beltz, R. McMeeking, F. Lange, *Science* **286**, 102 (1999).
21. A. Evans, Z. Suo, R. Wang, I. Aksay, M. He, J. Hutchinson, *J. Mater. Res.* **16**, 2476 (2001).
22. F. Song, A. Soh, Y. Bai, *Biomaterials* **24**, 3623 (2003).
23. F. Barthelat, H. Tang, P. Zavattieri, C. Li, H. Espinosa, *J. Mech. Phys. Solids* **55**, 306 (2007).
24. K. Okumura, P.-G. de Gennes, *Eur. Phys. J. E* **4**, 121 (2001).
25. K. Okumura, *Eur. Phys. J. E* **7**, 303 (2002).
26. P.-G. de Gennes, K. Okumura, *C. R. Acad. Sci., IV* **1**, 257 (2000).
27. K. Okumura, *J. Phys. Condens. Matter* **17**, S2879 (2005).
28. K. Okumura, *Europhys. Lett.* **63**, 701 (2003).
29. S. Kotha, Y. Li, N. Guzelsu, *J. Mater. Sci.* **36**, 2001 (2001).
30. D. Katti, K. Katti, J. Sopp, M. Sarikaya, *Comput. Theor. Polym. Sci.* **11**, 397 (2001).

https://doi.org/10.1557/mrs.2015.66 Published online by Cambridge University Press

31. B. Ji, H. Gao, *J. Mech. Phys. Solids* **52**, 1963 (2004).
32. P. Nukala, S. Zapperi, S. Šimunović, *Phys. Rev. E* **71**, 066106 (2005).
33. P. Fratzl, H. Gupta, F. Fischer, O. Kolednik, *Adv. Mater.* **19**, 2657 (2007).
34. T. Sumitomo, H. Kakisawa, Y. Owaki, Y. Kagawa, *J. Mater. Res.* **23**, 1466 (2008).
35. Y. Hamamoto, K. Okumura, *Phys. Rev. E* **78**, 026118 (2008).
36. Y. Aoyanagi, K. Okumura, *Phys. Rev. E* **79**, 066108 (2009).
37. Y. Hamamoto, K. Okumura, *Adv. Eng. Mater.* **15**, 522 (2013).
38. I.J. Beyerlein, S.L. Phoenix, A.M. Sastry, *Int. J. Solids Struct.* **33**, 2543 (1996).
39. S. Nakagawa, K. Okumura, *J. Phys. Soc. Jpn.* **76**, 4801 (2007).
40. Y. Aoyanagi, K. Okumura, *J. Phys. Soc. Jpn.* **78**, 034402 (2009).
41. H. Fabritius, C. Sachs, P. Triguero, D. Raabe, *Adv. Mater.* **21**, 391 (2009).
42. J. Weaver, G. Milliron, A. Miserez, K. Evans-Lutterodt, S. Herrera, I. Gallana, W. Mershon, B. Swanson, P. Zavattieri, E. DiMasi, D. Kisailus, *Science* **336**, 1275 (2012).
43. S. Nikolov, M. Petrov, L. Lymperakis, M. Friák, C. Sachs, H. Fabritius, D. Raabe, J. Neugebauer, *Adv. Mater.* **22**, 519 (2010).
44. C. Sachs, H. Fabritius, D. Raabe, *J. Mater. Res.* **21**, 1987 (2006).
45. T. Kato, A. Sugawara, N. Hosoda, *Adv. Mater.* **14**, 869 (2002).
46. Y. Yamamoto, T. Nishimura, A. Sugawara, H. Inoue, H. Nagasawa, T. Kato, *Cryst. Growth Des.* **8**, 4062 (2008).
47. A. Sugawara, T. Nishimura, Y. Yamamoto, H. Inoue, H. Nagasawa, T. Kato, *Angew. Chem. Int. Ed.* **45**, 2876 (2006).
48. K. Okumura, *J. Phys. Soc. Jpn.* **82**, 124802 (2013).
49. H. Gao, *Int. J. Solids Struct.* **27**, 1663 (1991).
50. S. Muju, *Compos. Sci. Technol.* **60**, 2213 (2000).
51. F. Fischer, J. Predan, P. Fratzl, O. Kolednik, *Int. J. Fract.* **173**, 57 (2012).
52. O. Kolednik, J. Predan, F. Fischer, P. Fratzl, *Adv. Funct. Mater.* **21**, 3634 (2011).
53. P.N. Witt, C.F. Reed, *Science* **149**, 1190 (1965).
54. P. Selden, *Nature* **340**, 711 (1989).
55. J.M. Gosline, M.W. Denny, M.E. DeMont, *Nature* **309**, 551 (1984).
56. F. Vollrath, D.T. Edmonds, *Nature* **340**, 305 (1989).
57. S. Osaki, *Nature* **384**, 419 (1996).
58. P.A. Guerette, D.G. Ginzinger, B.H. Weber, J.M. Gosline, *Science* **272**, 112 (1996).
59. F. Vollrath, D.P. Knight, *Nature* **410**, 541 (2001).
60. H.-J. Jin, D.L. Kaplan, *Nature* **424**, 1057 (2003).
61. O. Emile, A. Le Floch, F. Vollrath, *Nature* **440**, 621 (2006).
62. H. Zhou, Y. Zhang, *Phys. Rev. Lett.* **94**, 028104 (2005).
63. O. Emile, A. Le Floch, F. Vollrath, *Phys. Rev. Lett.* **98**, 167402 (2007).
64. W.M. Masters, *Behav. Ecol. Sociobiol.* **15**, 207 (1984).
65. L. Lin, D. Edmonds, F. Vollrath, *Nature* **373**, 146 (1995).
66. E. Wirth, F.G. Barth, *J. Comp. Physiol. A* **171**, 359 (1992).
67. M. Alam, M. Wahab, C. Jenkins, *Mech. Mater.* **39**, 145 (2007).
68. S. Cranford, A. Tarakanova, N. Pugno, M. Buehler, *Nature* **482**, 72 (2012).
69. T. Ackbarow, D. Sen, C. Thaulow, M.J. Buehler, *PLoS One* **4**, e6015 (2009).
70. M.J. Buehler, T. Ackbarow, *Mater. Today* **10**, 46 (2007).
71. Y. Aoyanagi, K. Okumura, *Phys. Rev. Lett.* **104**, 038102 (2010).
72. R. Emlet, *Biol. Bull.* **163**, 264 (1982).
73. J. Aizenberg, J. Weaver, M. Thanawala, V. Sundar, D. Morse, P. Fratzl, *Science* **309**, 275 (2005).
74. C.E. Hamm, R. Merkel, O. Springer, P. Jurkojc, C. Maier, K. Prechtel, V. Smetacek, *Nature* **421**, 841 (2003).
75. Y. Shiina, Y. Hamamoto, K. Okumura, *Europhys. Lett.* **76**, 588 (2006).
76. Y. Kashima, K. Okumura, *ACS Macro Lett.* **3**, 419 (2014).
77. N. Soné, M. Mori, K. Okumura, *J. Phys. Soc. Jpn.* **81**, 074604 (2012).
78. P.G. de Gennes, *Scaling Concepts in Polymer Physics* (Cornell University Press, New York, 1979).
79. P.-G. de Gennes, F. Brochard-Wyart, D. Quéré, *Gouttes, Bulles, Perles et Ondes* (Belin, Paris, 2nd ed. 2005).
80. M. Yokota, K. Okumura, *Proc. Natl. Acad. Sci. U.S.A.* **108**, 6395 (2011).
81. P.-G. de Gennes, *Rev. Mod. Phys.* **71**, S374 (1999).
82. Y. Takehara, K. Okumura, *Phys. Rev. Lett.* **112**, 148001 (2014). □

https://doi.org/10.1557/mrs.2015.66 Published online by Cambridge University Press